



# A comparative study of electropolymerization and photopolymerization for the determination of molnupiravir and their application in an electrochemical sensor via computationally designed molecularly imprinted polymers

Ahmet Cetinkaya<sup>1,2</sup> · M. Altay Unal<sup>3</sup> · Hasan Nazır<sup>4</sup> · M. Emin Çorman<sup>5</sup> · Lokman Uzun<sup>6</sup> · Sibel A. Ozkan<sup>1</sup>

Received: 11 January 2024 / Accepted: 5 April 2024  
© The Author(s) 2024

## Abstract

A comparative analysis of molecularly imprinted polymers based on different synthesis techniques was performed for the recognition of molnupiravir (MOL). The polymerizations were performed with 3-thienyl boronic acid (3-TBA) as a functional monomer by electropolymerization (EP) and with guanine methacrylate (GuaM) as a functional monomer by photopolymerization (PP). Morphological and electrochemical characterizations of the developed sensors were investigated to verify the constructed sensors. Moreover, quantum chemical calculations were used to evaluate changes on the electrode surface at the molecular and electronic levels. The dynamic linear range of both designed sensors under optimized experimental conditions was found to be  $7.5 \times 10^{-12}$ – $2.5 \times 10^{-10}$  M and  $7.5 \times 10^{-13}$ – $2.5 \times 10^{-11}$  M for EP and PP, respectively. The effect of various interfering agents on MOL peak current was assessed for the selectivity of the study. In the presence of 100 times more interfering agents, the RSD and recovery values were determined. The RSD values of GuaM/MOL@MIP/GCE and poly(Py-co-3-PBA)/MOL@MIP/GCE sensors were found to be 1.99% and 1.72%, respectively. Furthermore, the recovery values of the MIP-based sensors were 98.18–102.69% and 98.05–103.72%, respectively. In addition, the relative selectivity coefficient ( $k'$ ) of the proposed sensor was evaluated, and it exhibited good selectivity for MOL with respect to the NIP sensor. The prepared sensor was successfully applied to determine MOL in commercial serum samples and capsule form. In conclusion, the developed sensors provided excellent reproducibility, repeatability, high sensitivity, and selectivity against the MOL molecule.

**Keywords** Molnupiravir · Molecularly imprinted polymer · Electropolymerization · Photopolymerization · Modified electrode · Differential pulse voltammetry

## Introduction

The progression to severe symptoms and hospitalization can be significantly reduced with immediate care in confirmed COVID-19 patients with mild symptoms. Molnupiravir (MOL), a potent antiviral drug that may reduce the risk of hospitalization and death rates in non-hospitalized COVID-19 patients, was reported for the effective treatment for SARS-CoV-2 variants of concern (VoCs) [1–3]. The effectiveness statistics in COVID-19 patients have been extensively discussed [4–7]. MOL is an oral antiviral prodrug that has been approved to treat mild-to-moderate COVID-19 who are at high risk of developing severe disease. It has a wide range of preclinical efficacy against RNA viruses, including SARS-CoV-2 and its variations [8–10]. Using sensitive and trustworthy analytical techniques is necessary for the prior to investigating and determining.

✉ Sibel A. Ozkan  
sibel.ozkan@pharmacy.ankara.edu.tr

<sup>1</sup> Faculty of Pharmacy, Department of Analytical Chemistry, Ankara University, Ankara, Turkey  
<sup>2</sup> Graduate School of Health Sciences, Ankara University, Ankara, Turkey  
<sup>3</sup> Stem Cell Institute, Ankara University, Ankara, Turkey  
<sup>4</sup> Faculty of Science, Department of Chemistry, Ankara University, Ankara, Turkey  
<sup>5</sup> Gülhane Faculty of Pharmacy, Department of Biochemistry, University of Health Sciences, Ankara, Turkey  
<sup>6</sup> Faculty of Science, Department of Chemistry, Hacettepe University, Ankara, Turkey

In the recent literature, various analytical techniques such as high-performance liquid chromatography (HPLC) and reversed-phase HPLC [11, 12], liquid chromatography-tandem mass spectrometry (LC-MS-MS) [13–15], ultra-performance liquid chromatography-tandem mass spectrometry (UPLC-MS-MS) [16–18], high-performance thin-layer chromatography (HP-TLC) [17], UV-Vis [19], and fluorescent spectroscopy [20] have been reported for the quantification of MOL. The spectroscopy has some disadvantages, such as being only possible for analytes containing chromophores, strongly affected by pH, temperature, pollutants, and impurities, limited dynamic range, and lack of fluorescence of each molecule. However, one of the main drawbacks of chromatography is the high cost associated with the technique, as well as the time-consuming pre-processing steps involved. Electrochemical methods in contrast to chromatographic approaches provide shorter analysis times, minimize the use of organic solvents for green chemistry, and require simple sample preparation. These benefits make electrochemical methods a valuable alternative in various analytical settings, mainly where cost and time efficiency are important considerations. In this context, the determination of MOL using electrochemical methods is available in the more recent literature [21, 22]. However, molecularly imprinted electrochemical sensors have not yet been reported in the literature for the determination of MOL.

MIPs have gained significant attention as a promising technique for achieving excellent selectivity [23, 24]. The sensitivity of MIPs can be significantly improved by carefully considering and optimizing the polymer synthesis, experimental parameters, and surface modifications, which makes them more effective for various analytical and sensing applications [25]. MIPs offer numerous advantages in a wide range of applications with their high selectivity, cheap cost, and excellent chemical and thermal stability. MIPs have played a significant role in various industries and scientific disciplines [26, 27]. Electropolymerization (EP) and photopolymerization (PP) are frequently preferred in the development of functional polymers for drug analysis [23, 28–31]. Using pyrrole as a heteroaromatic monomer in EP demonstrates its suitability due to its biocompatibility and ease of polymerization [32, 33]. These techniques provide researchers powerful tools to create specialized detection systems and structures for drug analysis applications. However, the random orientation of the polymeric chain in this material causes poor adhesion and selectivity, which restrict utility of such kind of sensor systems [34]. Therefore, many different techniques have been proposed to produce copolymers to overcome these limitations and improve the performance of electrochemical sensors [23].

In this study, 3-thienyl boronic acid (3-TBA) and guanine methacrylate (GuaM) monomers were used separately as

functional monomers in EP and PP, respectively, to form MIP films with great selectivity and sensitivity for MOL. MIP films were synthesized using GuaM as a functional monomer with 2-hydroxyethyl methacrylate (HEMA), ethylene glycol dimethacrylate (EGDMA), the pore-forming agent polyvinyl pyrrolidone (PVP), and template molecule (MOL) in the PP technique. On the other hand, 3-TBA was polymerized with Py in the presence of MOL in the EP technique. Electrochemical impedance spectroscopy (EIS), cyclic voltammetry (CV), attenuated total reflectance-Fourier transform infrared (ATR-FTIR) spectroscopy, contact angle, and atomic force spectroscopy (AFM) were used to characterize the electrochemical and morphological characteristics of the poly(Py-co-3-TBA)/MOL@MIP/GCE and GuaM/MOL@MIP/GCE sensors. To determine MOL in both capsule form and commercial serum samples, the electrochemical capabilities of the sensors were thoroughly investigated. Furthermore, the template effect and the alterations to the electrode surface were discussed using theoretical calculations.

## Experimental section

### Chemicals and reagents

The detailed information for “chemicals and reagents” was supplied in the supplementary material.

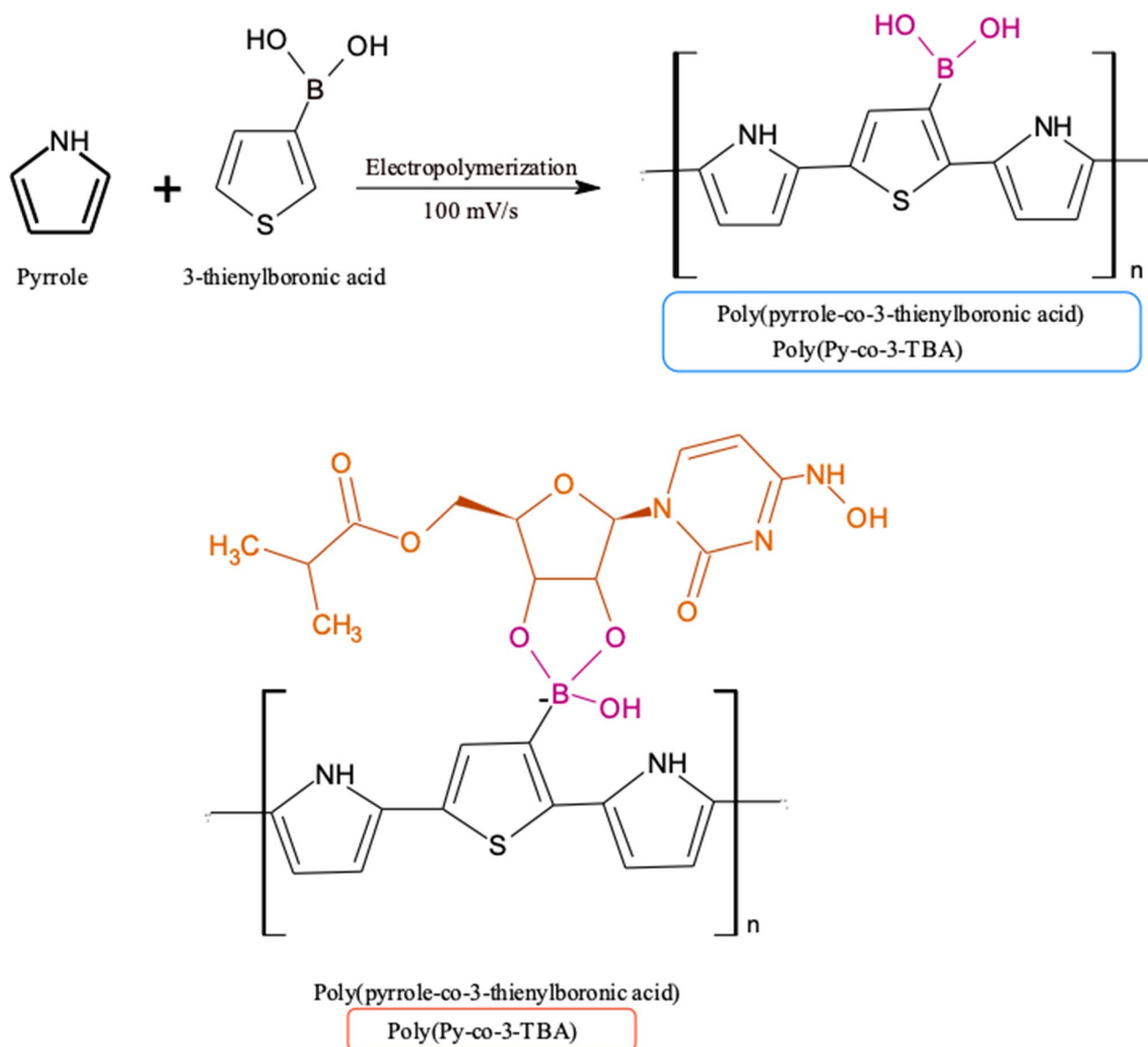
### Instrumentation

The detailed information for “instrumentation” is supplied in the supplementary material.

### Fabrication of the MIP- and NIP-based sensors

The glassy carbon electrode (GCE) was cleaned in methanol/water (1:1, v/v) under sonication for 10 min before each experiment. The alumina slurry was dropped onto the polishing pad before polishing the GCE and then rinsed with ultrapure water and dried at room temperature.

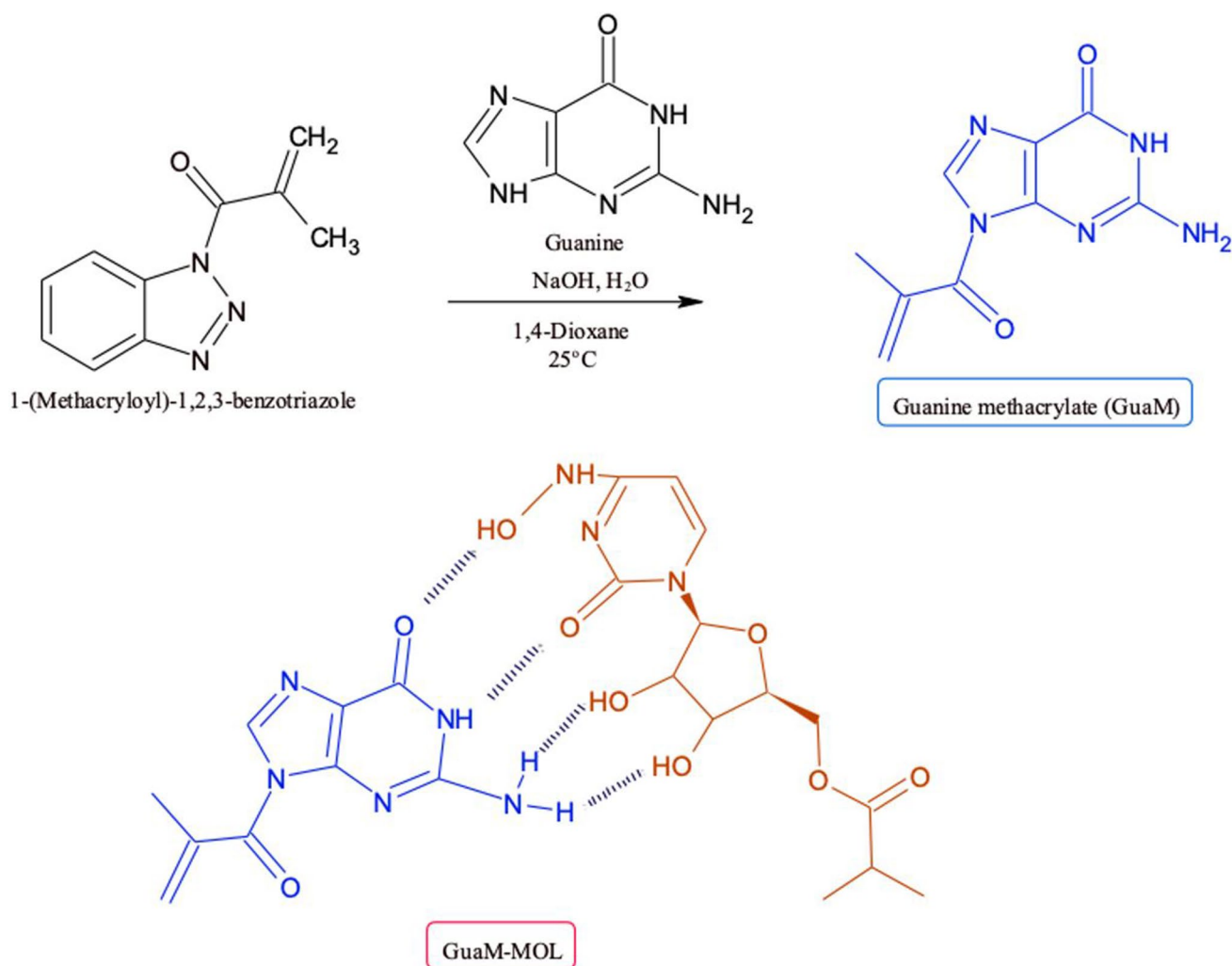
Py (0.05 M), 3-TBA (0.01 M), and MOL (0.01 M) were dissolved in phosphate-buffered solution (PBS, pH 7.5) containing LiClO<sub>4</sub> (0.1 M) as supporting electrolyte for the EP process (Scheme 1). The electrode was scanned for 10 cycles of CV from –0.2 to +1.6 at a scan rate of 100 mV/s (Figure S1). After polymerization was terminated, the film was washed by ultrapure distilled water. The template molecule was then removed using 7 cycles of CV in PBS (pH 7.5). Then, the electrodes were treated with MOL solution in known concentrations in the ThermoShaker at 500 rpm at 25°C for 10 min to rebind them to the exposed cavities.



**Scheme 1** Proposed interaction mechanism between 3-TBA and MOL

From the photopolymerization process, 1  $\mu\text{L}$  of TMSPMA solution was dropped onto the electrode surface and dried in the incubator at 50  $^{\circ}\text{C}$  for 10 min. The silane and methacrylate groups in TMSPM provide bonding between the polymeric film and the electrode surface, preventing the film from being removed from the surface. The PP solution was prepared as follows: homogen solution of pre-polymerization of MOL (0.01 M; template), and GuaM (0.01 M; functional monomer) (detailed information for GuaM synthesis was given in supplementary Materials), 100  $\mu\text{L}$  of HEMA (basic monomer), and 20  $\mu\text{L}$  of EGDMA (cross-linker) was stirred at R.T for 10 min.

Twenty microliters of the prepared polymerization solution was taken and 2  $\mu\text{L}$  of 2-hydroxy-2 methylpropisphenone was added (Scheme 2). Subsequently, 0.5  $\mu\text{L}$  of this mixture was dropped directly onto the surface of electrode and polymerization was performed by UV-induced free radical photopolymerization under UV light (100 W, 365 nm) for 5 min at room temperature under nitrogen atmosphere. The MOL template molecule was removed from polymeric coating using a ThermoShaker at 650 rpm at 25 $^{\circ}\text{C}$  for 10 min in the presence of the desorbing agent. Nonimprinted polymers (NIPs) were prepared for control studies using the same conditions without adding MOL.



**Scheme 2** A The synthesis route of GuaM and B proposed interaction mechanism between GuaM and MOL

### The commercial serum sample and capsule form applications

The detailed information for “[The commercial serum sample and capsule form applications](#)” is supplied in the supplementary material.

### Quantum chemical calculations

The detailed information for “quantum chemical calculations” is supplied in the supplementary material.

## Results and discussion

### Characterization of polymeric films

The developed sensors’ characterization results are illustrated in Fig. 1. Figure 1(a) displays the FT-IR spectra of

fic film for EP. The bands observed at 3110 due to N–H stretching vibration of Py ring and 2910  $\text{cm}^{-1}$  are assigned aromatic C–H stretching vibrations of Py and 3-TBA, respectively. The bands at around 1630, 1381, 1183, and 1049  $\text{cm}^{-1}$  are typical characteristics of the C=C bonds of thiophene ring, B–O stretching, B–O–H bending, and B–O–H deformation for 3-TBA (Fig. 1(a1)). On the other hand, Fig. 1(a2) presents the strong bands at 3335  $\text{cm}^{-1}$  and 1744  $\text{cm}^{-1}$  which correspond to O–H and C=O bonds due to inclusion of template molecule in the network of MIP as compared to NIP, which indicates the successful fabrication of NIP- and MIP-based electrochemical sensor films. In Fig. 1(b2), the bands observed for MIP films at 1070, 1154, and 1723  $\text{cm}^{-1}$  correspond to the –C–O, –C–O–C, and –C=O vibrations, respectively. Furthermore, a broadband around 3410  $\text{cm}^{-1}$  was stemmed from hydroxyl (–OH). The amide I, II, and III bands were seen at around 1594, 1486, and 1273  $\text{cm}^{-1}$ , which indicates that GuaM was successfully integrated into the polymeric network. The band observed at

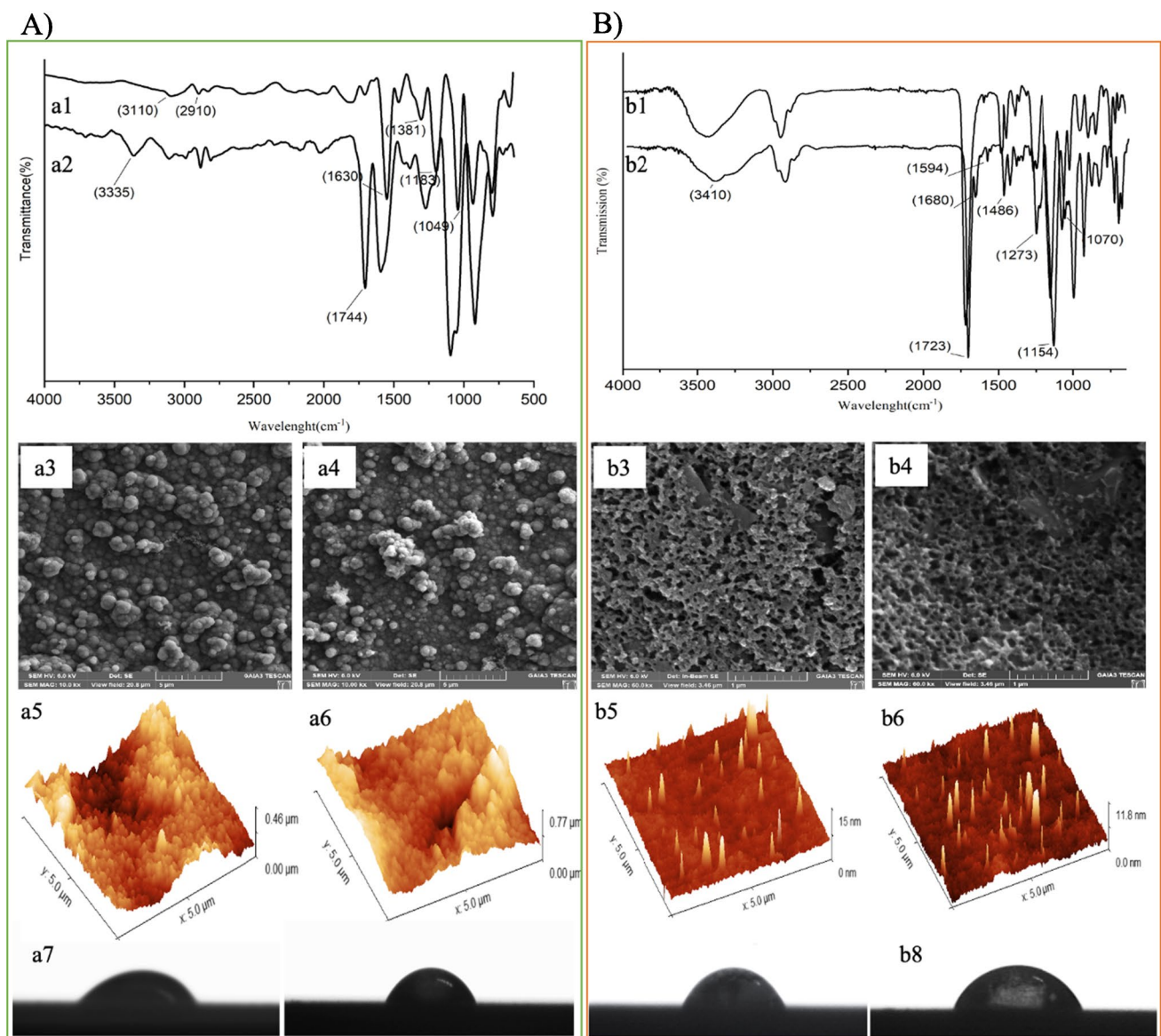


**Fig. 1** Characterizations of the electrode synthesized by EP **A** and PP **B**. ATR-FTIR spectra of NIP (a1, b1) and MIP (a2, b2); SEM images of MIP (a3, b3) and NIP (a4, b4); AFM images of MIP (a5, b5) and NIP (a6, b6). Contact angle of MIP (a7, b7) and NIP (a8, b8)

1680 cm<sup>-1</sup> differed, which may be due to the presence of the target molecule in the MIP compared to the NIP (Fig. 1(b2)). When comparing monomers and polymeric chain, for EP and PP, the longer conjugated polymer chain exhibits better symmetry and greater equilibrium electron density than the monomer, and the adsorption peaks of the bond shift to higher/lower wavenumbers (supplementary material S3). As displayed in Fig. 1(a3), the MIP film exhibits a dense and irregular arrangement of particles. Besides, the SEM images of NIP appear to have similar shapes, which is expected as they are synthesized under the same conditions. On the other hand, porous structures were observed for fabricated electrodes synthesized by PP process (Fig. 1(b3, b4)) due to

the removal of a sacrificial agent of PVP compared to the electrode synthesized by the EP process. Figure 1(a5, a6, b5, b6) presents typical AFM images of fabricated sensors. The surface deepness for MIP and NIP surfaces were taken as 0.46 μm and 0.77 μm for EP, whereas those were determined as 8.4 nm and 9.8 nm for PP, respectively. These results showed that film formation was successfully achieved and is also well fitted to the results of SEM images. These results also confirm that surface roughness was increased for electrodes synthesized by EP due to the polymerization cycles compared to PP. The contact angle measurement is shown in Fig. 1(a7, a8, b7, b8). The contact angle values obtained on electrode synthesized by EP was 60.5 and 65.0° for MIP and

NIP, respectively, while the contact angle value synthesized by PP was 70.5° and 72.8° for MIP and NIP, respectively. The MIP film exhibited a relatively higher hydrophilicity than NIP due to the character of MIPs recognition cavities.

### Electrochemical characterizations of MIP surfaces

The “supplementary materials” file includes “Electrochemical characterizations of MIP surfaces” for this section.

### Optimization of the parameters of the designed sensors

The “supplementary materials” file includes in the detail the “[Optimization of the parameters of the designed sensors](#)” for this section.

The parameters of the sensors developed using EP and PP techniques were optimized. Based on the  $\Delta I$  values obtained with both EP and PP, the monomer:template ratio of 1:1 was selected as the optimal value for both sensors in order to generate the most stable and effective polymers. In the EP process, the CV technique was used to create a durable and useful polymeric film. After selecting appropriate monomers and ratios to provide a polymer with the required stability and thickness, the optimal number of EP cycles was found to be 10 cycles. The PP time under UV lamp was optimized, and 0.25  $\mu\text{L}$  of polymerization solution was dropped and exposed to UV light for different periods of time to form a stable polymeric layer on the GCE surface, achieving good reproducible and stable polymerization in 5 min. Appropriate removal solutions were used for both EP and PP. In the EP method, the best peak current value was obtained in PBS solution with pH 7.5 as removal solutions. CV approach was used to remove template molecules after different cycles and the best result was achieved after 7 cycles and this removal solution was used in all steps. In the PP method, 5 M HAc was used as the removal solution. Additionally, different removal times were evaluated and 10 min was chosen as the optimum removal time due to the most stable and reproducible results. In the PP method, 5 M HAc was used as the removal solution. Additionally, different removal times were evaluated and 10 min was chosen as the optimum removal time due to the most stable

**Table 1** The significant optimization parameters for EP and PP

	poly(Py-co-3-TBA)/MOL@MIP/GCE (EP)	GuaM/MOL@MIP/GCE (PP)
Monomer:template ratio	1:1	1:1
Dropping volume ( $\mu\text{L}$ )		0.25
PP time (min)		5
Number of cycles for EP	10	
Removal solution	pH 7.5 PBS	5 M HAc
Number of cycles for Removal	7	
Removal time (min)		10
Rebinding time (min)	10	20

and reproducible results. To evaluate its effect on rebinding to MIP-based sensors prepared for both EP and PP, the rebinding solution was applied for different times and examined with the help of ThermoShaker (500 rpm, 25°C). When the difference between the peak currents after reconnection and removal was evaluated, the highest peak current values were selected at 10 min for EP and 20 min for PP. The parameters given in Table 1 were optimized to obtain the best poly(Py-co-3-TBA)/MOL@MIP/GCE and GuaM/MOL@MIP/GCE sensors.

### Assessment of analytical performance of poly(Py-co-3-TBA)/MOL@MIP/GCE and GuaM/MOL@MIP/GCE sensors

The analytical performance of the poly(Py-co-3-TBA)/MOL@MIP/GCE sensor was assessed by the measurement of MOL in the linear concentration range between  $7.5 \times 10^{-12}$  M and  $2.5 \times 10^{-10}$  M (Fig. 2B). The regression equation was calculated in this concentration range as  $\Delta I (\mu\text{A}) = 1.80 \times 10^{11} (\mu\text{A}/\text{M}) \times C(\text{M}) + 44.44$  ( $r = 0.996$ ) using 5.0 mM  $[\text{Fe}(\text{CN})_6]^{3-/4-}$  solution as the redox probe by indirect measurements. The results of the regression parameters are summarized in Table 1. The LOD and LOQ values were  $6.01 \times 10^{-13}$  M and  $2.00 \times 10^{-12}$  M, respectively. The LOD and LOQ values were obtained using theoretical calculation methods in the ICH Guidelines. They were calculated based on the “Standard Deviation of the Response and the Slope” method in the ICH Guidelines using the following equations [35, 36]:

$$\text{LOD} \left( \text{LOD} = 3 \times \frac{\text{standard deviation}}{\text{slope}} \right) \text{ and } \text{LOQ} \left( \text{LOQ} = 10 \times \frac{\text{standard deviation}}{\text{slope}} \right)$$

The results showed excellent sensitivity from the poly(Py-co-3-TBA)/MOL@MIP/GCE sensor. Under ideal conditions, the proposed sensor was used to identify MOL using the DPV method (Fig. 2A). The performance of the

NIP-based sensor was also investigated using poly(Py-co-3-TBA)/MOL@NIP/GCE to determine MOL over the studied concentration range. The MIP curve (red color) showed a linear response with  $\Delta I$  increasing proportional to MOL

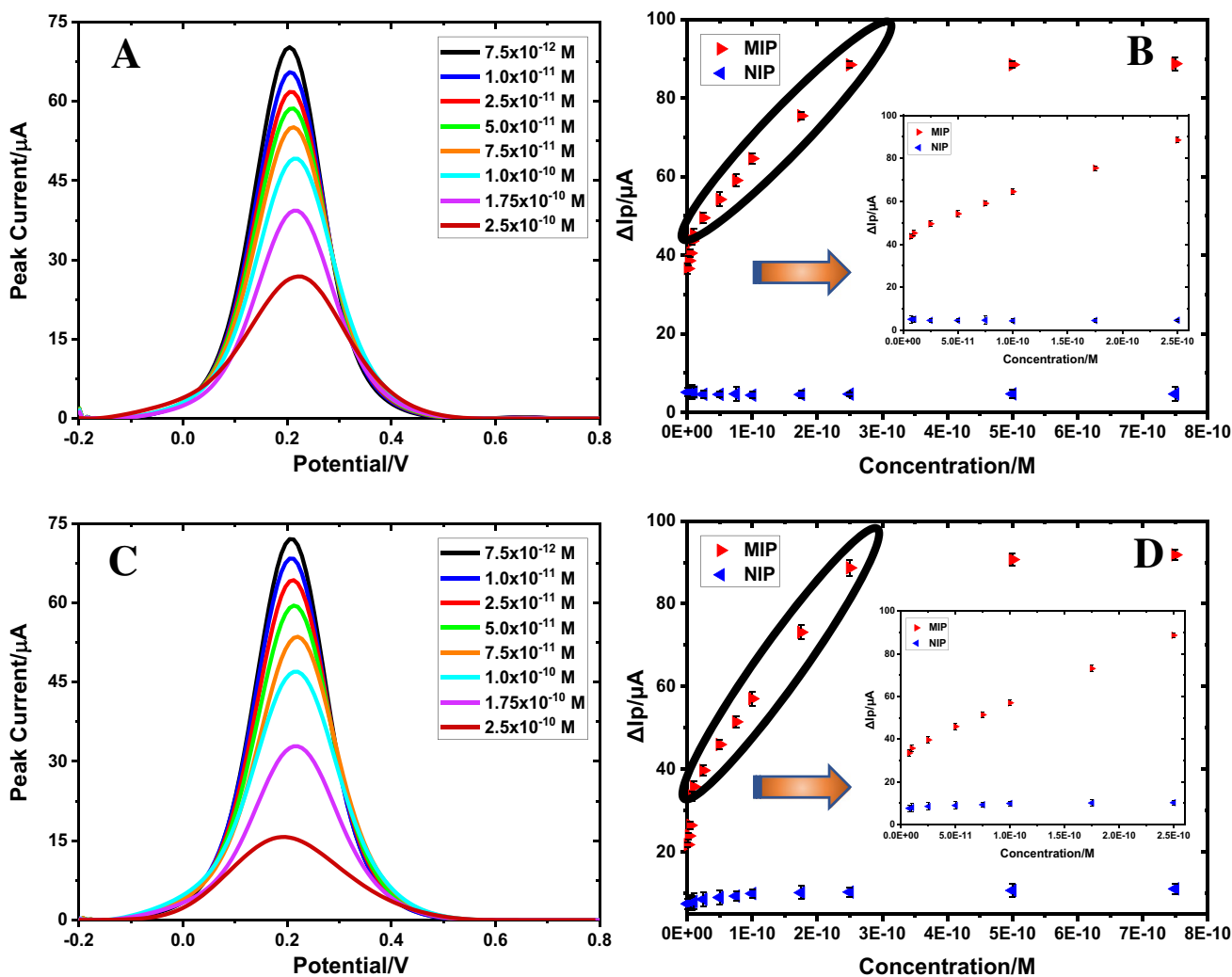


**Fig. 2** DPV voltammograms obtained after rebinding of various MOL concentrations in standard solution (A) and commercial serum solution (C), calibration curve for poly(Py-co-3-TBA)/MOL@MIP/

GCE in standard solution (B), commercial serum solution (D) (in 5 mM  $[\text{Fe}(\text{CN})_6]^{3-/4-}$  solution (0.1 M KCl))

concentration, but no linearity was observed for NIP. The NIP curve (blue color) exhibited a small  $\Delta I$  value, in contrast to MIP, because there were no NIP-specific recognition sites for MOL. These results indicated the poly(Py-co-3-TBA)/MOL@MIP/GCE sensor has good sensitivity and selectivity for MOL detection.

The analytical performance of the GuaM/MOL@MIP/GCE sensor was evaluated under ideal experimental conditions with the DPV method using range of MOL concentrations from  $7.5 \times 10^{-13}$  M to  $2.5 \times 10^{-11}$  M (Table 2). The regression equation was found to be as  $\Delta I$  ( $\mu\text{A}$ ) =  $1.86 \times 10^{12}$  ( $\mu\text{A}/\text{M}$ )  $\times C$  (M) + 39.11 ( $r = 0.996$ ), and the GuaM/MOL@MIP/GCE sensor displayed a linear response for selective and sensitive MOL detection. The calculated values for the LOD and LOQ were

$1.13 \times 10^{-13}$  M and  $3.76 \times 10^{-13}$  M, respectively. The NIP-based sensor measured selectivity (blue color) and controlled analytical performance in the same concentration range as the MOL. The relationship between declining  $[\text{Fe}(\text{CN})_6]^{3-/4-}$  peaks and rising MOL concentrations is seen in Fig. 3A. The results show good selectivity and sensitivity of GuaM/MOL@MIP/GCE for MOL detection. The plots of MOL concentration versus  $\Delta I$  values for MIP and NIP-based sensors are given in Fig. 3B. The findings demonstrate the superior selectivity and sensitivity of GuaM/MOL@MIP/GCE for detecting MOL. Compared to poly(Py-co-3-TBA)/MOL@MIP/GCE, GuaM/MOL@MIP/GCE showed a porous structure and a thinner layer, enabling the detection of MOL at lower concentrations.

**Table 2** Regression parameters of MOL on poly(Py-co-3-TBA)/MOL@MIP/GCE and GuaM/MOL@MIP/GCE sensors

	EP		PP	
	Standard solution	Serum sample	Standard solution	Serum sample
Linearity range (M)	$7.5 \times 10^{-12}$ – $2.5 \times 10^{-10}$	$7.5 \times 10^{-12}$ – $2.5 \times 10^{-10}$	$7.5 \times 10^{-13}$ – $2.5 \times 10^{-11}$	$7.5 \times 10^{-13}$ – $2.5 \times 10^{-11}$
Slope ( $\mu\text{A}/\text{M}$ )	$1.80 \times 10^{11}$	$2.23 \times 10^{11}$	$1.86 \times 10^{12}$	$1.95 \times 10^{12}$
SE of slope	$6.49 \times 10^{10}$	$4.89 \times 10^{10}$	$6.74 \times 10^{10}$	$4.28 \times 10^{10}$
Intercept ( $\mu\text{A}$ )	44.44	33.84	39.11	28.87
SE of intercept	0.77	0.58	0.80	0.51
Correlation coefficient ( <i>r</i> )	0.996	0.999	0.996	0.998
LOD (M)	$6.01 \times 10^{-13}$	$1.79 \times 10^{-12}$	$1.13 \times 10^{-13}$	$6.93 \times 10^{-14}$
LOQ (M)	$2.00 \times 10^{-12}$	$5.97 \times 10^{-12}$	$3.76 \times 10^{-13}$	$2.31 \times 10^{-13}$
Repeatability of peak current (RSD%)*	1.07	1.23	0.89	1.11
Reproducibility of peak current (RSD%)*	1.76	1.83	1.62	1.97

\*Each value is the mean of three experiments

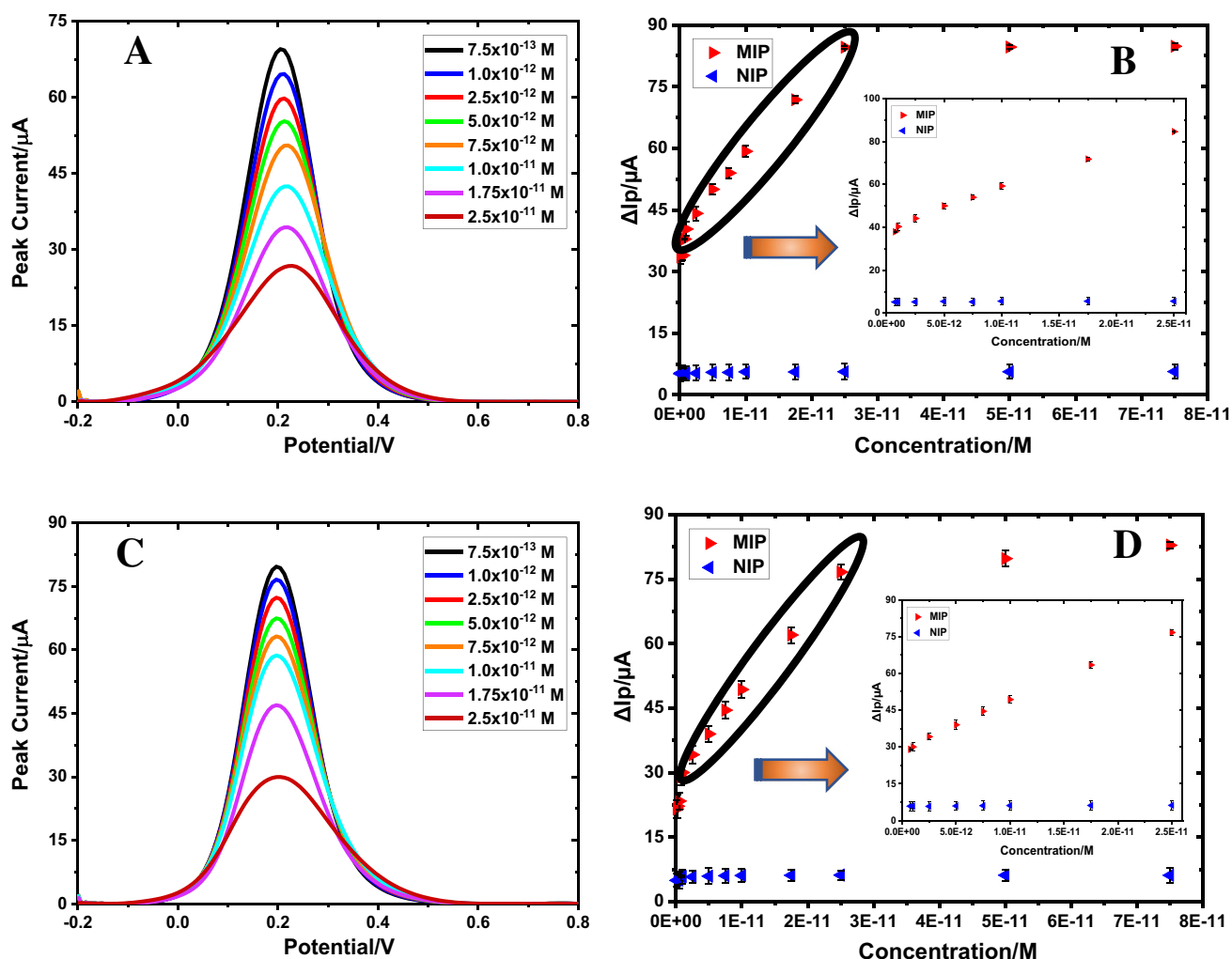


**Fig. 3** DPV voltammograms obtained after rebinding of various MOL concentrations in standard solution **A** and commercial serum solution **C**, calibration curve for GuaM/MOL@MIP/GCE in standard

solution, **B** commercial serum solution **D** (in 5 mM  $[\text{Fe}(\text{CN})_6]^{3-/4-}$  solution, 0.1 M KCl)



## Application of the developed sensors to commercial serum samples and capsule form

The analysis of MOL has been applied successfully to capsule form and commercial serum samples with the poly(Py-co-3-TBA)/MOL@MIP/GCE and GuaM/MOL@MIP/GCE sensors. The sensor showed excellent performance in complicated matrices with high sensitivity, specificity, and accuracy in the determination (Table 3). The known amounts of the analyte were added to samples during the recovery studies, and the poly(Py-co-3-TBA)/MOL@MIP/GCE and GuaM/MOL@MIP/GCE sensors were used to measure the concentration of the analyte in the samples. The recovery studies were very satisfactory with excellent recovery percentages and RSD values and given in Table 3. The measurements were made with diluted solutions from stock solutions prepared as described in section S1.3. The quantities found without adding known analyte concentrations are given in Table 3 below the label quantity. The findings were found to be consistent with the MOL amount mentioned in the capsule form and commercial serum samples. The MIP-based sensor prepared using the EP method showed a linear response with a proportional increase in  $\Delta I$  with MOL concentration according to DPV data for serum samples. In contrast, the NIP-based sensor showed no significant change in  $\Delta I$  compared to MIP (Fig. 2C, D). The recovery values of the poly(Py-co-3-TBA)/MOL@MIP/GCE sensor for capsule form and commercial serum samples were found as 101.35% and 99.09%, respectively (Table 3). This demonstrated the applicability of the designed sensor for real samples.

Similarly, the MOL was first spiked in capsule form and commercial serum samples at certain concentrations in PP and analyzed with the developed GuaM/MOL@MIP/GCE sensor and results are given in Fig. 3C and D. The recovery percentages were calculated as 99.40% and 100.97%,

respectively (Table 3). These findings also demonstrate that the GuaM/MOL@MIP/GCE sensor has been successfully used in real samples.

The Student  $t$ - and  $F$ -tests were used to statistically evaluate the validity of the results obtained from the poly(Py-co-3-TBA)/MOL@MIP/GCE and GuaM/MOL@MIP/GCE sensors. The experimentally obtained Student  $t$ - and  $F$ -test values at the 95% confidence level are lower than the theoretically stated Student  $t$ - and  $F$ -tests, demonstrating the relevance of these two recommended sensors in MOL studies.

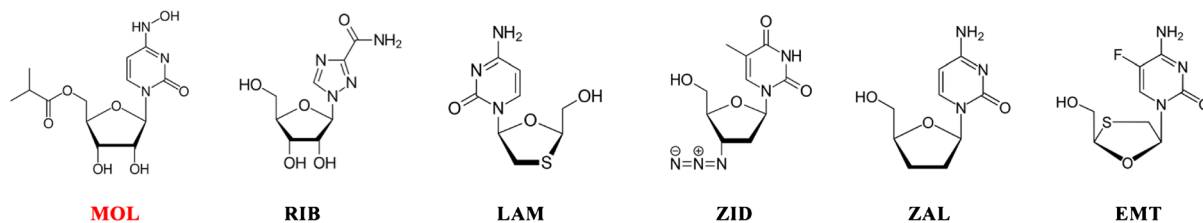
## Selectivity studies

The ability to achieve greater selectivity and affinity for the target molecule is the main benefit of integrating MIPs into electrochemical sensors. To emphasize this benefit and demonstrate the sensor's selectivity in comparison to other compounds with comparable structures (such as ribavirin (RIB), lamivudine (LAM), zidovudine (ZID), zalcitabine (ZAL), and emtricitabine (EMT)), *relative selectivity coefficient* ( $k'$ ) tests were conducted. The ratio of the  $\Delta I$  values of the template molecule (MOL) to those of the competing drugs (RIB, LAM, ZID, ZAL, and EMT) was used to calculate the selectivity coefficient ( $k$ ) value. The selectivity coefficients of MOL for MIP/GCE and NIP/GCE were also calculated to estimate the relative selectivity coefficient ( $k'$ ), which indicates the specific recognition capability gained by MIPs (Table 4). "The selectivity coefficient ( $k$ ) is defined as the ratio between current value for template and structurally analog drugs as follows:  $k = \text{current value}_{\text{template}} / \text{current value}_{\text{competitor}}$  shows that selectivity ( $k$ ) found for MOL was greater; this implies that MIP has relatively better binding tendencies with template MOL as compared to other compounds. The relative selectivity coefficient ( $k'$ ) can be defined as expressed in Eq.  $k' = k_{\text{MIP}} / k_{\text{NIP}}$  (Table 4).

**Table 3** Recovery results for MOL for capsule form and serum samples

	EP		PP	
	Capsule form	Serum sample	Capsule form	Serum sample
Label amount (mg)	200.000	–	200.000	–
Found amount (mg)*	201.778	–	199.013	–
RSD%	1.97	–	1.24	–
Bias%	-0.89	–	0.49	–
Calculated $t_{\text{value}}$	0.22			
Calculated $F_{\text{value}}$	0.38			
Spiked amount (mg)	10.000	10.000	10.000	10.000
Found amount (mg)*	10.135	9.909	9.940	10.097
Average recovery (%)	101.35	99.09	99.40	100.97
RSD%	1.50	1.56	1.87	1.60
Bias%	-0.14	0.91	0.60	-0.97

\*Each value is the mean of five experiments. Theoretical Student  $t$  and  $F$  values are 2.13 and 6.38, respectively

**Table 4** Selectivity values of MOL and other similar drug substances

Compound	EP					PP				
	MIP/GCE		NIP/GCE			MIP/GCE		NIP/GCE		
	$\Delta I/\mu A$	$k_{(MIP)}$	$\Delta I/\mu A$	$k_{(NIP)}$	$k'_{(MIP/NIP)}$	$\Delta I/\mu A$	$k_{(MIP)}$	$\Delta I/\mu A$	$k_{(NIP)}$	$k'_{(MIP/NIP)}$
<b>MOL</b>	54.21	-	4.58	-	-	55.02	-	5.68	-	-
<b>RIB</b>	27.47	1.97	9.12	0.50	3.94	22.62	2.21	10.29	0.55	4.02
<b>LAM</b>	16.37	3.31	7.57	0.61	5.43	10.77	4.64	8.49	0.67	6.93
<b>ZID</b>	18.22	2.98	8.60	0.53	5.62	12.35	4.05	9.63	0.59	6.86
<b>ZAL</b>	21.15	2.56	10.75	0.42	6.10	11.34	4.41	9.55	0.60	7.35
<b>EMT</b>	21.63	2.51	11.08	0.41	6.12	12.14	4.12	10.09	0.55	7.49

This equation allows an estimation of the effect of imprinting on selectivity which measure the identification capability and selectivity of the MIPs for template with respect to NIPs [23, 29, 37]. A high  $k'$  value confirmed that the imprinting process was achieved successfully and provided specific recognition sites toward MOL based on the size and shape of the template's molecules. According to these values, poly(Py-co-3-TBA)/MOL@MIP/GCE specifically recognized MOL molecules by 3.94-, 5.43-, 5.62-, 6.10-, and 6.12-fold corresponding to RIB, LAM, ZID, ZAL, and EMT, respectively. For the GuaM/MOL@MIP/GCE, these values were calculated as 4.02-, 6.93-, 6.86-, 7.35-, and 7.49-fold for RIB, LAM, ZID, ZAL, and EMT, respectively. Also, the  $k'$  values were greater than 1.0, which is the threshold value for indicating resolution between the target and competitor molecules." As a result, both poly(Py-co-3-TBA)/MOL@MIP/GCE and GuaM/MOL@MIP/GCE surfaces exhibited higher selectivity toward MOL than RIB, LAM, ZID, ZAL, and EMT compared to NIP surfaces. GuaM/MOL@MIP/GCE also displayed greater selectivity for MOL than poly(Py-co-3-TBA)/MOL@MIP/GCE.

### Interference studies

The performance of MIP-based sensors can be affected by various substances present in biological fluids, such as  $K^+$ ,  $Cl^-$ ,  $Na^+$ ,  $SO_4^{2-}$ , dopamine (DA), ascorbic acid (AA), uric acid (UA), and paracetamol (PAR) in the serum matrix. The MOL concentrations employed for the selectivity test were  $5.0 \times 10^{-11}$  M and  $5.0 \times 10^{-12}$  M, respectively, in the poly(Py-co-3-TBA)/MOL@MIP/GCE and GuaM/MOL@MIP/GCE sensors. The RSD and recovery values were calculated in

the presence of 100 times more interfering agents. Hereby, RSD values for poly(Py-co-3-PBA)/MOL@MIP/GCE and GuaM/MOL@MIP/GCE sensors were determined as 1.72% and 1.99%, respectively. Additionally, the MIP-based sensors' recovery values were found to be 98.18–102.69% and 98.05–103.72%, respectively (Fig. 4). These results demonstrated that interfering substances showed low or no effect on the effectiveness of sensors designed for MOL detection.

### Quantum chemical calculations

The structures of the MOL, 3-TBA, and GuaM molecules used in this study (A), the calculated optimized structure (B), and the electrostatic potential (ESP) charge distribution on the surface of the molecule (C) were subjected to quantum chemical calculations in order to evaluate the applicability of the sensors (Figures S5-S6-S7). Additionally, computer computational analysis of MOL has two stable conformations: keto oxime and hydroxyl oxime [38]. The calculations for these molecules are given in Figure S5-III and Figure S5-IV, respectively. Molecules are polar, as seen on ESP maps (red, electronegative; blue, electropositive). As a result, they can serve as electron donors and acceptors, or they can create non-covalent or hydrogen bonds. Additionally, it appears that MOL's stable conformations are polar (Figure S5-III and Figure S5-IV). On the other hand, it can be concluded from a comparison of the energy levels of the compounds (Fig. 5) that the addition of 3-TBA and Py [23] to MOL (1:5:1) raises the energy level of the high-occupied molecular orbital (HOMO) (from  $-6.680$  to  $-5.942$  eV). The GuaM contribution (1:1) also increased the HOMO energy level from  $-6.680$  to  $-6.226$  eV, whereas it decreased the LUMO

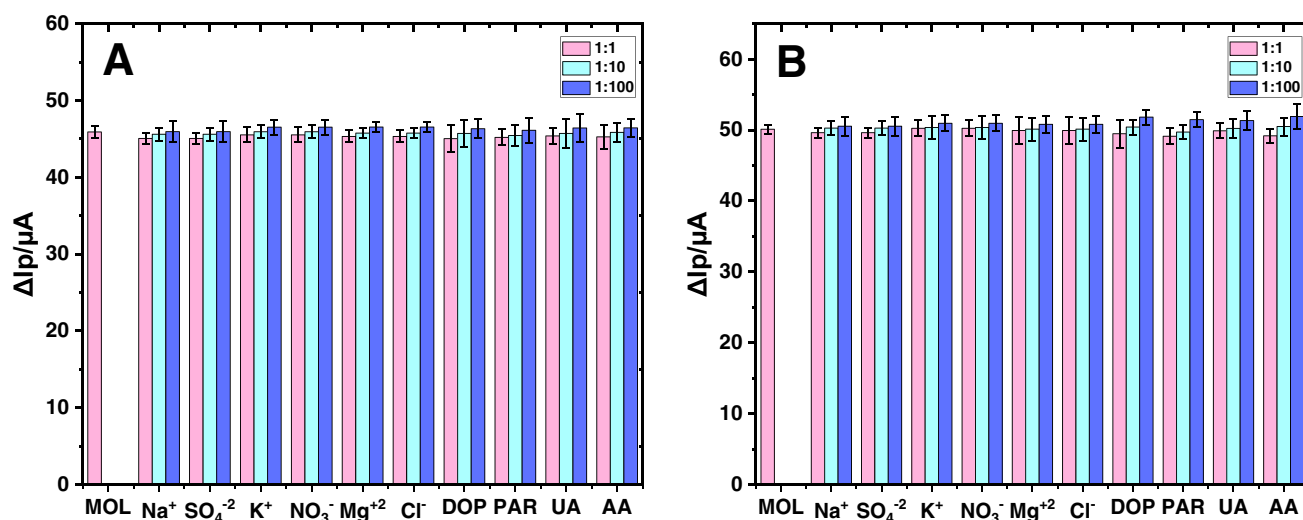


**Fig. 4** Bar graphs of **A**  $5.0 \times 10^{-11}$  M MOL at poly(Py-co-3-TBA)/MOL@MIP/GCE; **B**  $5.0 \times 10^{-12}$  M MOL at GuaM/MOL@MIP/GCE in the presence of interfering agents at 1:1, 1:10, and 1:100 ratio using 5 mM  $[\text{Fe}(\text{CN})_6]^{3-/4-}$  redox probe

energy level from  $-1.570$  to  $-2.238$  eV. This means that the monomers used show HOMO and LUMO dope properties against MOL. On the other hand, when the stable

conformations of MOL are taken into consideration, it is seen that these properties do not change. However, the novel polymeric forms (poly(Py-co-3-TBA)/MOL@MIP/GCE

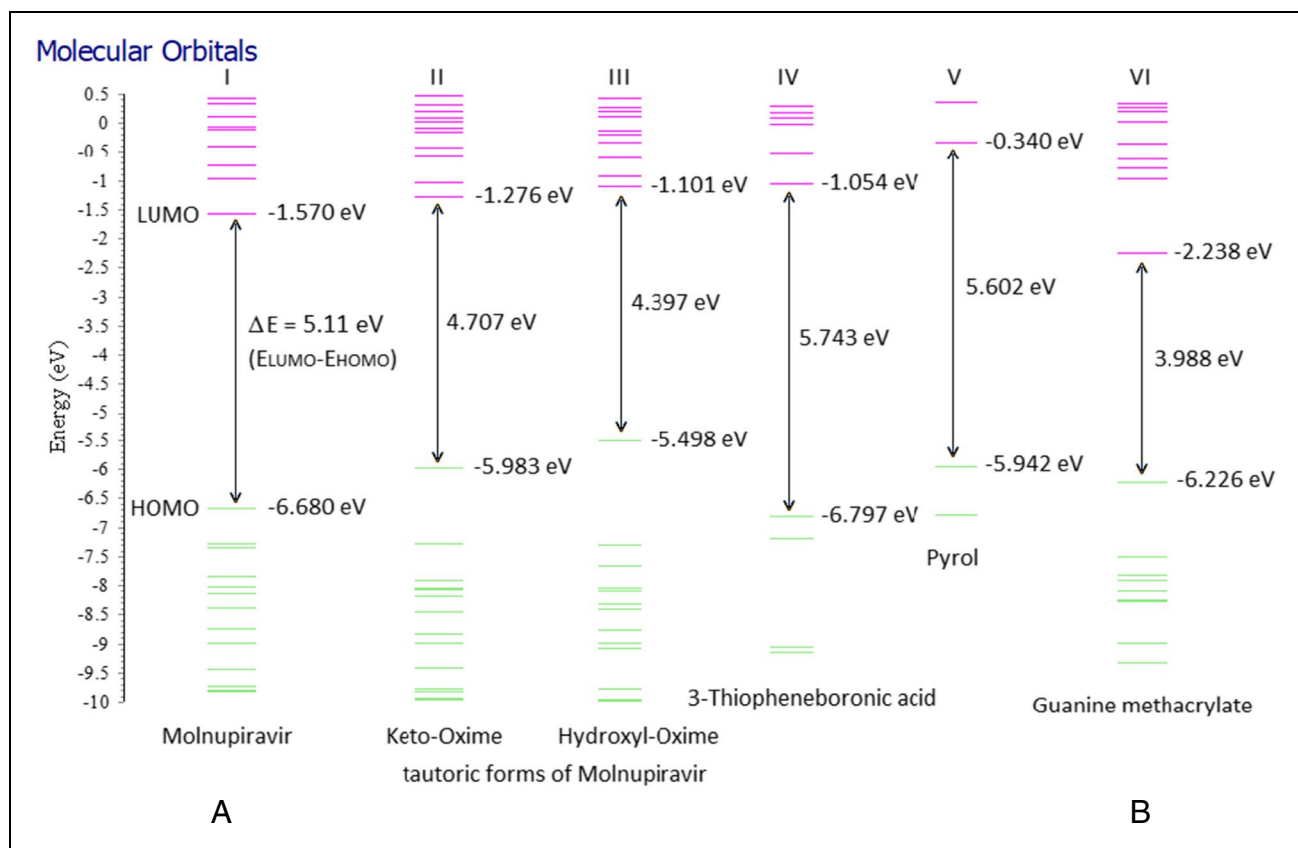


**Fig. 5** Comparison of HOMO–LUMO molecular orbital energy diagrams. **A**  $\Delta E_{(\text{LUMO-HOMO})}$  energy of trio MOL(I, II, and III), 3-TBA (IV) and Py (V) =  $3.928$  eV [23]. **B**  $\Delta E_{(\text{LUMO-HOMO})}$  energy of duo MOL(I, II, and III) and GuaM (VI) =  $3.260$  eV

and GuaM/MOL@MIP/GCE) have higher electron mobilities due to the smaller band gap, which makes the template effect determination easier. In Table S1, molecules' computed electronic, energetic, and geometric descriptor values are presented. According to the first view, MOL molecules have bigger geometric descriptor values for SASA (solvent accessible surface area) and SA (surface area) than other molecules, which will cause their solubility in the polymeric matrix to occur more quickly. Additionally, the findings of the calculations for a molecule's solubility (LogS) (Table S1) and electronic descriptors (absolute electronegativity,  $\chi$ ; extra electronic charge from the environment, and  $\Delta N_{\text{max}}$ ) were consistent. On the other hand, electronegativity causes areas of positive and negative charge to form on the surface of the molecule, and this induced charge has an impact on the molecule's solubility in solvents. Thus, as solvent-molecule polar-polar interactions grow, a polar molecule dissolves readily in a polar solvent. MOL is more soluble because it has stronger polar SASA and SA values than other molecules. Additionally, MOL's hydrophobicity descriptor LogP is smaller than that of other molecules, suggesting that MOL is more hydrophilic and dissolves more quickly as a result. On the other hand, the poly(Py-co-3-TBA)/MOL@MIP pair's docking calculation with Py reveals that up to 5 Py molecules can be attached to the structure (Fig. 6 and Figure S8), supporting the findings of the experiment (Figure S3A). The ideal GuaM/MOL@

MIP form ratio was likewise determined to be 1:1 (Figure S9), which was also supported by an experiment (Figure S4A) (MOL-GuaM; 1:2,  $E = -74668.127477$  eV; 1:1,  $E = -53644.244489$  eV). This finding demonstrates that a 1:2 increase in stability results in an unacceptable reduction in the MOL's resolution (Figure S9).

## Comparison with other methods

The "Comparison with other methods" is included in the "supplementary materials" file for this section.

## Conclusion

In this study, different types of MIP-based sensors were constructed for detection of MOL in standard solution, capsule form, and commercial serum samples. Py and 3-TBA monomers were co-polymerized to create the poly(Py-co-3-TBA)/MOL@MIP/GCE sensor for EP, while GuaM and HEMA were co-polymerized to create the GuaM/MOL@MIP/GCE sensor for PP. The poly(Py-co-3-TBA)/MOL@MIP/GCE sensor showed shortest response time that of the GuaM/MOL@MIP/GCE sensor when optimization parameters were taken into account. However, GuaM/MOL@MIP/GCE sensor showed better performance for the LOD, LOQ, repeatability, reproducibility, and reusability than the poly(Py-co-3-TBA)/MOL@MIP/GCE sensor. Furthermore, commercial serum samples and capsule forms were used to test the applicability of the created sensors. The accuracy and usefulness of the sensors were demonstrated by the recovery and %RSD values. The selectivity was calculated using the  $k'$  values of the substances with similar drugs. Additionally, sensor's selectivity was not impacted by the presence of interfering agents at a concentration 100 times that of the target molecule. As a result of the stability studies, the sensor developed by EP method was stable for 2 days, while the sensor prepared by PP method was stable for 5 days. In light of these data, it can be concluded that the sensor created for MOL using PP has a better stability.

The accuracy of the sensors created using quantum chemical calculations was thoroughly discussed, and electrochemical and morphological characterizations confirmed MIP-based sensors. As a result, the GuaM/MOL@MIP/GCE sensor compared to poly(Py-co-3-TBA)/MOL@MIP/GCE offered significant advantages such as linear range, LOD and LOQ values, stability, reusability, excellent selectivity, and easy applicability. The accuracy of sensors created using quantum chemical calculations was investigated.

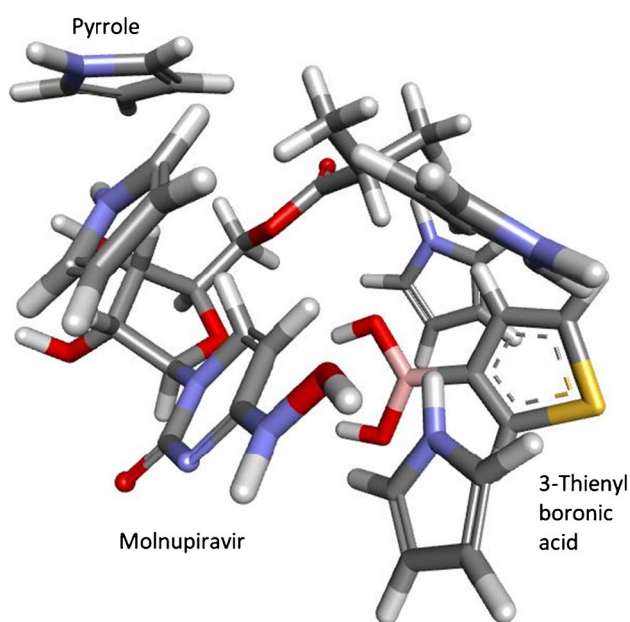


**Fig. 6** Schematic representation of the molecular docking results of five pyrroles around the poly(Py-co-3-TBA)/MOL complex

**Supplementary Information** The online version contains supplementary material available at <https://doi.org/10.1007/s00604-024-06353-w>.

**Acknowledgements** This work was produced as a part of Ahmet Cetinkaya's Ph.D. thesis. Ahmet Cetinkaya thanks the financial support from the Council of Higher Education 100/2000 (YOK) under the special 100/2000 scholarship program and the Scientific and Technological Research Council of Turkey (TUBITAK) under the BIDEB/2211-A Ph.D. and ARDEB/1004 Ph.D. Scholarship Programs.

**Author contribution** Ahmet Cetinkaya: conceptualization; methodology; software; writing—original draft; validation; investigation. M. Altay Unal: investigation, resources, data curation, writing—original draft. Hasan Nazır: data curation, resources, DFT calculation, writing—original draft. M. Emin Çorman: investigation, data curation, resources, writing—original draft. Lokman Uzun: supervision, writing—review and editing. Sibel A. Ozkan: supervision; writing—review and editing; project administration.

**Funding** Open access funding provided by the Scientific and Technological Research Council of Türkiye (TÜBİTAK).

**Data availability** The datasets generated during and/or analyzed during the current study are available from the corresponding author on reasonable request.

## Declarations

**Ethical approval** This study does not require any ethical approval.

**Conflict of interest** The authors declare no competing interests.

**Open Access** This article is licensed under a Creative Commons Attribution 4.0 International License, which permits use, sharing, adaptation, distribution and reproduction in any medium or format, as long as you give appropriate credit to the original author(s) and the source, provide a link to the Creative Commons licence, and indicate if changes were made. The images or other third party material in this article are included in the article's Creative Commons licence, unless indicated otherwise in a credit line to the material. If material is not included in the article's Creative Commons licence and your intended use is not permitted by statutory regulation or exceeds the permitted use, you will need to obtain permission directly from the copyright holder. To view a copy of this licence, visit <http://creativecommons.org/licenses/by/4.0/>.

## References

- Holman W, Holman W, McIntosh S et al (2021) Accelerated first-in-human clinical trial of EIDD-2801/MK-4482 (molnupiravir), a ribonucleoside analog with potent antiviral activity against SARS-CoV-2. *Trials* 22:561. <https://doi.org/10.1186/s13063-021-05538-5>
- Gordon CJ, Tchesnokov EP, Schinazi RF, Götte M (2021) Molnupiravir promotes SARS-CoV-2 mutagenesis via the RNA template. *J Biol Chem* 297(1):10770. <https://doi.org/10.1016/j.jbc.2021.100770>
- Abdelnabi R, Foo CS, De Jonghe S et al (2021) Molnupiravir inhibits replication of the emerging SARS-CoV-2 variants of concern in a hamster infection model. *J Infect Dis* 224:749–753. <https://doi.org/10.1093/infdis/jiab361>
- Malone B, Campbell EA (2021) Molnupiravir: coding for catastrophe. *Nat Struct Mol Biol* 28:706–708
- Kabinger F, Stiller C, Schmitzová J et al (2021) Mechanism of molnupiravir-induced SARS-CoV-2 mutagenesis. *Nat Struct Mol Biol* 28:740–746. <https://doi.org/10.1038/s41594-021-00651-0>
- Abdelnabi R, Foo CS, Kaptein SJF, et al (2021) The combined treatment of molnupiravir and favipiravir results in a potentiation of antiviral efficacy in a SARS-CoV-2 hamster infection model. *EBio-Medicine* 72:103595. <https://doi.org/10.1016/j.ebiom.2021.103595>
- Khoo SH, Fitzgerald R, Fletcher T et al (2021) Optimal dose and safety of molnupiravir in patients with early SARS-CoV-2: a phase I, open-label, dose-escalating, randomized controlled study. *J Antimicrob Chemother* 76:3286–3295. <https://doi.org/10.1093/jac/dkab318>
- Wahl A, Gralinski LE, Johnson CE et al (2021) SARS-CoV-2 infection is effectively treated and prevented by EIDD-2801. *Nature* 591:451–457. <https://doi.org/10.1038/s41586-021-03312-w>
- Sheahan TP, Sims AC, Zhou S, et al (2020) An orally bioavailable broad-spectrum antiviral inhibits SARS-CoV-2 in human airway epithelial cell cultures and multiple coronaviruses in mice. *Sci Transl Med* 12(541):eabb5883. <https://doi.org/10.1126/scitranslmed.abb5883>
- Cetinkaya A, Kaya SI, Ozkan SA (2023) A comprehensive overview of sensors applications for the diagnosis of SARS-CoV-2 and of Drugs Used in its Treatment. *Crit Rev Anal Chem* 1–21. <https://doi.org/10.1080/10408347.2023.2186693>
- Reçber T, Timur SS, Erdoğan Kablan S, et al (2022) A stability indicating RP-HPLC method for determination of the COVID-19 drug molnupiravir applied using nanoformulations in permeability studies. *J Pharm Biomed Anal* 30(214):114693. <https://doi.org/10.1016/j.jpba.2022.114693>
- Annadi AM, El Zahar NM, Abdel-Sattar NE-DA et al (2022) Development and validation of molnupiravir assessment in bulk powder and pharmaceutical formulation by the RP-HPLC-UV method. *RSC Adv* 12:34512–34519. <https://doi.org/10.1039/d2ra05066h>
- Parsons TL, Kryszak LA, Marzinke MA (2021) Development and validation of assays for the quantification of  $\beta$ -D-N4-hydroxycytidine in human plasma and  $\beta$ -D-N4-hydroxycytidine-triphosphate in peripheral blood mononuclear cell lysates. *J Chromatogr B Analyt Technol Biomed Life Sci* 1182:122921. <https://doi.org/10.1016/j.jchromb.2021.122921>
- Amara A, Penchala SD, Else L, et al (2021) The development and validation of a novel LC-MS/MS method for the simultaneous quantification of Molnupiravir and its metabolite  $\beta$ -D-N4-hydroxycytidine in human plasma and saliva. *J Pharm Biomed Anal* 206:114356. <https://doi.org/10.1016/j.jpba.2021.114356>
- Gouda AS, Marzouk HM, Rezk MR, et al (2022) A validated LC-MS/MS method for determination of antiviral prodrug molnupiravir in human plasma and its application for a pharmacokinetic modeling study in healthy Egyptian volunteers. *J Chromatogr B Analyt Technol Biomed Life Sci* 1206:123363. <https://doi.org/10.1016/j.jchromb.2022.123363>
- Chang C-H, Peng W-Y, Lee W-H, et al (2023) Transfer and biotransformation of the COVID-19 prodrug molnupiravir and its metabolite  $\beta$ -D-N4-hydroxycytidine across the blood-placenta barrier. *EBio Medicine* 95:104748. <https://doi.org/10.1016/j.ebiom.2023.104748>
- Saraya RE, El DS, Salman BI, Ibrahim AE (2022) Highly sensitive high-performance thin-layer chromatography method for the simultaneous determination of molnupiravir, favipiravir, and ritonavir in pure forms and pharmaceutical formulations. *J Sep Sci* 45:2582–2590. <https://doi.org/10.1002/jssc.202200178>
- Sharaf YA, El Deeb S, Ibrahim AE, et al (2022) Two green micellar HPLC and mathematically assisted UV spectroscopic methods for the simultaneous determination of molnupiravir

- and favipiravir as a novel combined COVID-19 antiviral regimen. *Molecules* 27(7):2330. <https://doi.org/10.3390/molecules27072330>
19. Abdelazim AH, Abourehab MAS, Abd Elhalim LM, et al (2023) Green adherent spectrophotometric determination of molnupiravir based on computational calculations; application to a recently FDA-approved pharmaceutical dosage form. *Spectrochim Acta A Mol Biomol Spectrosc* 285:121911. <https://doi.org/10.1016/j.saa.2022.121911>
  20. Younis HM, Youssef AO, El-Sheikh SM et al (2023) Preparation and characterization of Fe-gallic acid MOF for determination of antiviral molnupiravir as inhibitor for RNA corona virus replication. *Microchem J* 194:109297. <https://doi.org/10.1016/j.microc.2023.109297>
  21. Kablan SE, Reçber T, Tezel G, et al (2022) Voltammetric sensor for COVID-19 drug molnupiravir on modified glassy carbon electrode with electrochemically reduced graphene oxide. *J Electroanal Chem* 920:116579. <https://doi.org/10.1016/j.jelechem.2022.116579>
  22. Vural K, Karakaya S, Dilgin DG, et al (2023) Voltammetric determination of Molnupiravir used in treatment of the COVID-19 at magnetite nanoparticle modified carbon paste electrode. *Microchem J* 184:108195. <https://doi.org/10.1016/j.microc.2022.108195>
  23. Cetinkaya A, Unal MA, Nazir H, et al (2023) Two different molecularly imprinted polymeric coating techniques for creating sensitive and selective electrochemical sensors for the detection of Ribavirin. *Sens Actuators B Chem* 389:133914. <https://doi.org/10.1016/j.snb.2023.133914>
  24. Sulym I, Cetinkaya A, Yence M, et al (2022) Novel electrochemical sensor based on molecularly imprinted polymer combined with L-His-MWCNTs@PDMS-5 nanocomposite for selective and sensitive assay of tetracycline. *Electrochim Acta* 430:141102. <https://doi.org/10.1016/j.electacta.2022.141102>
  25. Uzun L, Turner APF (2016) Molecularly-imprinted polymer sensors: realising their potential. *Biosens Bioelectron* 76:131–144. <https://doi.org/10.1016/j.bios.2015.07.013>
  26. Çorman ME, Özcelikay G, Cetinkaya A, et al (2022) Metal-organic frameworks as an alternative smart sensing platform for designing molecularly imprinted electrochemical sensors. *TrAC - Trends Anal Chem* 150:116573. <https://doi.org/10.1016/j.trac.2022.116573>
  27. Kaya SI, Cetinkaya A, Ozkan SA (2022) Latest advances in determination of bisphenols with nanomaterials, molecularly imprinted polymers and aptamer based electrochemical sensors. *Crit Rev Anal Chem* 52:1223–1243. <https://doi.org/10.1080/10408347.2020.1864719>
  28. Cetinkaya A, Bilge S, Karadurmus L et al (2022) The role and the place of ionic liquids in molecularly imprinted polymer-based electrochemical sensors development for sensitive drug assay. *TrAC - Trends Anal Chem* 147:116512. <https://doi.org/10.1016/j.trac.2021.116512>
  29. Cetinkaya A, Kaya SI, Atici EB et al (2022) A semi-covalent molecularly imprinted electrochemical sensor for rapid and selective detection of tiotropium bromide. *Anal Bioanal Chem* 414(28):8023–8033. <https://doi.org/10.1007/s00216-022-04335-6>
  30. Cetinkaya A, Kaya SI, Çorman ME et al (2022) A highly sensitive and selective electrochemical sensor based on computer-aided design of molecularly imprinted polymer for the determination of leflunomide. *Microchem J* 179:107496. <https://doi.org/10.1016/j.microc.2022.107496>
  31. Yamani HZ, El Azab NF (2024) First electropolymerized carbodopa-based molecularly imprinted film: disposable electrochemical sensor for monitoring of anti-COVID-19 drug favipiravir in human plasma. *Microchem J* 196:109572. <https://doi.org/10.1016/j.microc.2023.109572>
  32. Domínguez-Renedo O, Navarro-Cuñaño AM, Arnáiz-Lozano V, Alonso-Lomillo MA (2020) Molecularly imprinted polypyrrole based electrochemical sensor for selective determination of 4-ethylphenol. *Talanta* 207:120351. <https://doi.org/10.1016/j.talanta.2019.120351>
  33. Wang F, Zhu L, Zhang J (2014) Electrochemical sensor for levofloxacin based on molecularly imprinted polypyrrole-graphene-gold nanoparticles modified electrode. *Sens Actuators B Chem* 192:642–647. <https://doi.org/10.1016/j.snb.2013.11.037>
  34. Maziz A, Özgür E, Bergaud C, Uzun L (2021) Progress in conducting polymers for biointerfacing and biorecognition applications. *Sensors Actuators Rep* 3:100035. <https://doi.org/10.1016/j.snr.2021.100035>
  35. Ozkan SA, Kauffmann J-M, Zuman P (2015) *Electroanalysis in biomedical and pharmaceutical sciences*. Springer Berlin Heidelberg, Berlin, Heidelberg. <https://doi.org/10.1007/978-3-662-47138-8>
  36. Validation of analytical procedures: Text and methodology. International Conference on Harmonisation (ICH) Guideline (1995)
  37. Kaya SI, Cetinkaya A, Atici EB, et al (2022) Electrochemical sensing of acridinium bromide with metal ion-assisted molecularly imprinted films. *Microchem J* 184:108128. <https://doi.org/10.1016/j.microc.2022.108128>
  38. Sharov A V., Burkhanova TM, Tok TT, et al (2022) Computational analysis of molnupiravir. *Int J Mol Sci* 23(3):1508. <https://doi.org/10.3390/ijms23031508>

**Publisher's Note** Springer Nature remains neutral with regard to jurisdictional claims in published maps and institutional affiliations.